In Vivo Imaging of Immuno-Spin Trapped Radicals With Molecular Magnetic Resonance Imaging in a Diabetic Mouse Model

Rheal A. Towner,[1] Nataliya Smith,[1] Debra Saunders,[1] Michael Henderson,[1] Kristen Downum,[1] Florea Lupu,[2] Robert Silasi-Mansat,[2] Dario C. Ramirez,[3] Sandra E. Gomez-Mejiba,[3] Marcelo G. Bonini,[4] Marilyn Ehrenshaft,[5] and Ronald P. Mason[5]

Oxidative stress plays a major role in diabetes. In vivo levels of membrane-bound radicals (MBRs) in a streptozotocin-induced diabetic mouse model were uniquely detected by combining molecular magnetic resonance imaging (mMRI) and immunotrapping techniques. An anti-DMPO (5,5-dimethyl-1-pyrroline *N*-oxide) antibody (Ab) covalently bound to an albumin (BSA)-Gd (gadolinium)-DTPA (diethylene triamine penta acetic acid)-biotin MRI contrast agent (anti-DMPO probe), and mMRI, were used to detect in vivo levels of DMPO-MBR adducts in kidneys, livers, and lungs of diabetic mice, after DMPO administration. Magnetic resonance signal intensities, which increase in the presence of a Gd-based molecular probe, were significantly higher within the livers, kidneys, and lungs of diabetic animals administered the anti-DMPO probe compared with controls. Fluorescence images validated the location of the anti-DMPO probe in excised tissues via conjugation of streptavidin-Cy3, which targeted the probe biotin moiety, and immunohistochemistry was used to validate the presence of DMPO adducts in diabetic mouse livers. This is the first report of noninvasively imaging in vivo levels of MBRs within any disease model. This method can be specifically applied toward diabetes models for in vivo assessment of free radical levels, providing an avenue to more fully understand the role of free radicals in diabetes. ***Diabetes*** **61:2405–2413, 2012**

Oxidative stress plays a crucial role in diabetes (1,2). Long-term exposure to oxidative stress is strongly implicated in the pathogenesis of multiple organs from diabetes, such as the liver, kidneys, and heart (3). Protein damage results as a consequence of oxidative stress in diabetes (4). Streptozotocin (STZ), which destroys the insulin-producing β-cells of the pancreas (5), has been used as a type 1 diabetes model in rodents by numerous investigators for several decades. In an STZ-induced diabetes model in rats, an increase in the carbonyl modification of proteins has been previously detected in the liver and kidneys (6).

It would be advantageous to understand the extent and timing of these oxidative stress processes in vivo by specifically monitoring free radical–related events. To date, in vivo imaging of free radicals has been challenging and has resulted in limited applications. Nitroxyl radicals, which are paramagnetic, can be detected with electron paramagnetic resonance (EPR) imaging (EPRI) directly, with Overhauser magnetic resonance imaging (MRI) or MRI indirectly (7), or by applying EPR/nuclear magnetic resonance (NMR) coimaging (8), to provide in vivo redox imaging information. EPRI was previously used to assess oxidative stress in rat renal diseases (9), including diabetes (10). A study involving targeted tumor-specific probes, incorporated nitroxides encapsulated into anti-human epidermal growth factor receptor 2 (HER2) immunoliposomes that could be visualized with EPRI (11). Nitroxyl radicals can couple with reactive oxygen species (ROS) and subsequently become diamagnetic species. Disadvantages of this technique are that nitroxyl radicals can easily be bioreduced by reductases and ascorbic acid, a wide variety of radicals react with nitroxyl radicals (i.e., nonspecific), and positive detection of radicals results in a loss in the paramagnetic effect (e.g., loss of EPR signal or a loss in contrast effect in MRI). Fluorescence multiphoton imaging in isolated organs (e.g., kidneys) (12), or use of quantum dots in cells (13), has been used to image alterations in cellular redox states, but these applications are not well suited for whole-body imaging. Recently, use of hyperpolarized ^{13}C-dehydroascorbate and ^{13}C-NMR spectroscopy has been reported as an endogenous redox sensor for in vivo metabolic imaging (14).

Molecular MRI (mMRI) relies on the specific labeling of extracellular cell-surface receptors or antigens with a targeted contrast agent containing an antibody (Ab) or peptide. These antibody targeting probes alter proton magnetization relaxation times at their sites of accumulation, making them ideal for diagnostic purposes. Magnetic resonance (MR) contrast agents, such as paramagnetic, gadolinium (Gd)-based contrast agents, generate a positive signal contrast (T_1 contrast), which enhances MR signal intensities of water molecules that surround the Gd-based contrast agents in T_1-weighted MRIs. Gd-based compounds, bound to affinity molecules, are increasingly used for mMRI.

In this study we report the in vivo imaging of membrane-bound radicals (MBR) for the first time. A novel approach involves the use of mMRI and immuno-spin trapping to monitor levels of reactive free radicals in oxidative stress-related diseases. For instance, protein and bound lipid

From the [1]Advanced Magnetic Resonance Center, Oklahoma Medical Research Foundation, Oklahoma City, Oklahoma; the [2]Cardiovascular Biology Research Program, Oklahoma Medical Research Foundation, Oklahoma City, Oklahoma; the [3]Experimental Therapeutics Research Laboratory, Oklahoma Medical Research Foundation, Oklahoma City, Oklahoma; the [4]Section of Cardiology, Department of Pharmacology, University of Illinois, Chicago, Illinois; and the [5]Laboratory of Pharmacology and Chemistry, National Institute of Environmental Health Sciences, Research Triangle Park, North Carolina.

Corresponding author: Rheal A. Towner, rheal-towner@omrf.org.

Received 2 November 2011 and accepted 5 April 2012.

DOI: 10.2337/db11-1540

D.C.R. and S.E.G.-M. are now affiliated with the Laboratory of Experimental and Therapeutic Medicine-IMIBIO-SL-CONICET and the Department of Molecular Biology National University of San Luis, San Luis, Argentina.

radicals that are generated as a result of oxidative stress processes can be trapped by the spin-trapping compound, 5,5-dimethyl-1-pyrroline *N*-oxide (DMPO), to form DMPO-MBR adducts (see Fig. 1*A*), which can be further assessed by immuno-spin trapping, a method that uses an Ab against the DMPO-nitrone adduct (15). With the use of molecular imaging technology, it is possible to monitor in vivo formation of oxidative products resulting from free radicals in real time within a rodent disease model of oxidative stress, such as diabetes. Therefore, the combined morphologic image resolution of mMRI, the use of a gadolinium (Gd)-DTPA (diethylene triamine penta acetic acid)-albumin–based contrast agent (see Fig. 1*B* for compound illustration) for signal detection, and the specificity of Abs for protein/lipid radicals (anti-DMPO Ab, which binds to DMPO-protein/lipid adducts resulting from oxidative-stress-induced formation of protein/lipid radicals), was used to detect in vivo oxidative stress–related processes (see Fig. 1*C* for experimental strategy for targeting of DMPO-protein/lipid adducts). The anti-DMPO probe was assessed in an experimental STZ-induced mouse model for diabetes, after the trapping of MBR with DMPO. In this study, mMRI assessments focused on the liver, kidney, and lung regions, which are all organs that undergo diabetes-associated pathologies.

RESEARCH DESIGN AND METHODS

Syntheses of DMPO-specific MRI contrast agents. To recognize the DMPO-MBR adducts, a mouse monoclonal anti-DMPO Ab was used. The macromolecular contrast material, biotin-BSA-Gd-DTPA, was prepared as previously described (16–18). A solution of biotin-BSA-Gd-DTPA was added directly to the solution of Ab (anti-DMPO, 200 μg/mL) for conjugation through a sulfo-NHS (*N*-hydroxysuccinimide)-EDC (N,N-(3-dimethylaminopropyl)-N'-ethyl-carbodiimide hydrochloride) link between albumin and the Ab, as previously

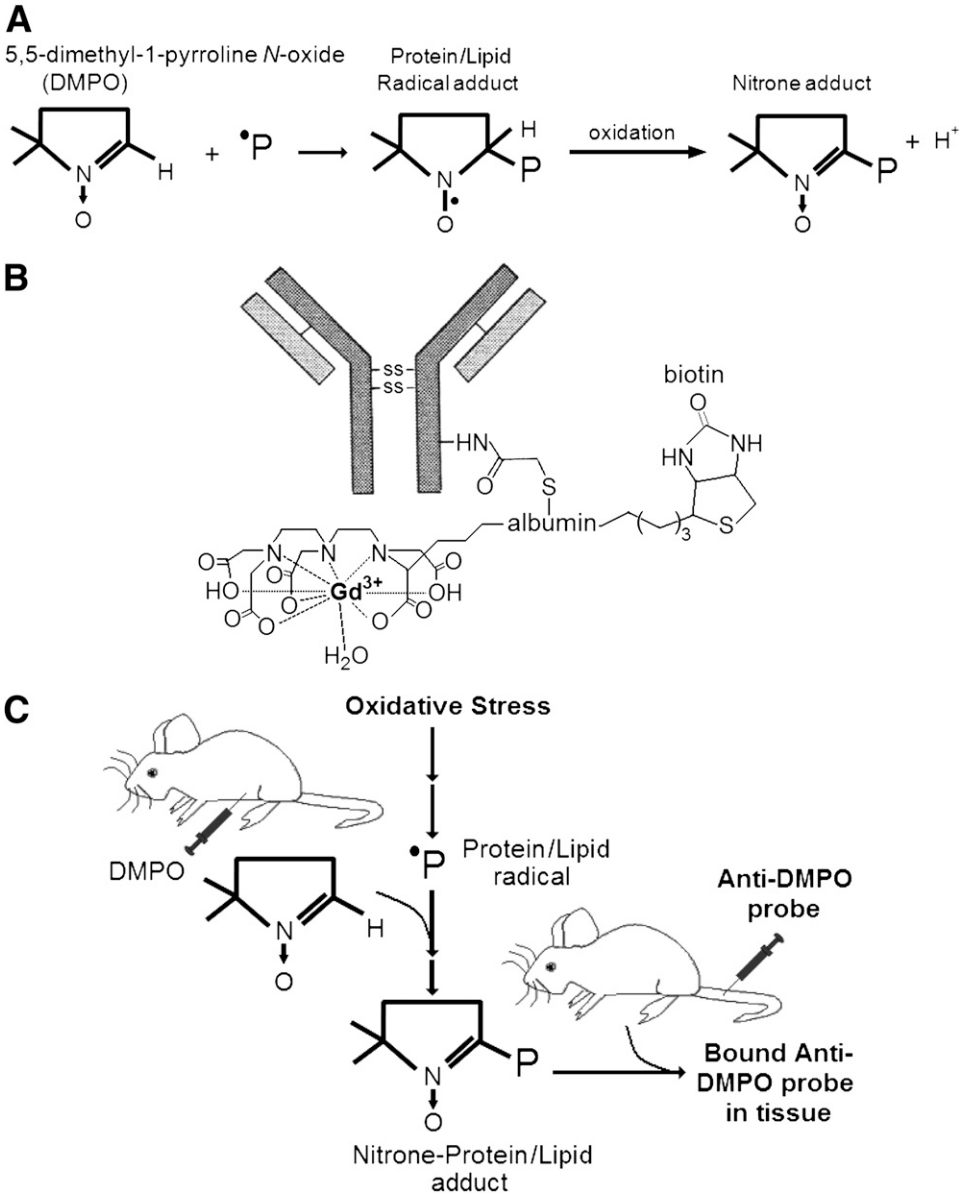

FIG. 1. Schematic description of in vivo imaging of bound protein and lipid radicals. *A*: Trapping of protein and membrane-bound lipid radicals with DMPO. The short-lived protein/lipid radical adduct can be assessed by ESR spectroscopy, or the long-lived nitrone adduct can be assessed by immunotrapping. *B*: Illustration of the anti–DMPO-albumin-Gd-DTPA-biotin mMRI probe. *C*: Immunotrapping of protein/lipid radicals ($^{\bullet}$P) with anti-DMPO mMRI probe. DMPO is injected intraperitoneally to trap protein/lipid radicals and generate nitrone-protein/lipid adducts. Anti-DMPO is injected intravenously to target nitrone-protein/lipid adducts, which can be visualized in vivo by mMRI.

described (16–18). The product was lyophilized, stored at 4°C, and reconstituted to a desirable concentration for injections in PBS. The final amount of the product, anti-DMPO-biotin-BSA-Gd-DTPA that was injected into mice is estimated to be 20 μg anti-DMPO Ab/injection and 10 mg biotin-BSA-Gd-DTPA/injection. The molecular weight of the anti-DMPO-biotin-BSA-Gd-DTPA probe is estimated to be 232 kDa. We estimate there are 1.3 biotin and 23 Gd-DTPA groups bound to each BSA molecule. As a control, normal rat-IgG (healthy rat; Apha Diagnostic International, San Antonio, TX) conjugated to biotin-BSA-Gd-DTPA (IgG contrast agent) was synthesized by the same protocol.

STZ-induced diabetes model. C57BL/6J mice (n = 20; aged 6–8 weeks) were treated with STZ (100 mg/kg intraperitoneally daily for 2 days), and were assessed for glucose levels between 4 and 6 weeks. Mice were considered diabetic if glucose levels were >250–300 mg/dL. Diabetes was characterized as severe when glucose levels were >300 mg/dL (n = 5) and as moderate when glucose levels were between 250 and 300 mg/dL (n = 5). To test for glucose, a drop of blood from the tail was put on a testing strip and read on a Bayer Ascensia Elite XL glucometer. For control groups, (1) some diabetic mice were not given DMPO but were injected with saline (non-DMPO control; n = 5), (2) nondiabetic mice were given DMPO (nondisease control; n = 5), or (3) other diabetic mice were given DMPO, but administered the nonspecific IgG contrast agent (contrast agent control) instead of the anti-DMPO probe (n = 5). DMPO administration started at 7 weeks after STZ treatment. Mice were administered the anti-DMPO probe at 8 weeks after STZ treatment.

DMPO administration. DMPO (25 μL in 100 μL saline) was administered intraperitoneally three times daily (every 6 h) for 5 days (i.e., 0.42 μL DMPO/μL saline daily). Administration of DMPO was initiated in mice 7 weeks after STZ administration, before injection of the anti-DMPO probe.

MR techniques. For the MR experiments, mice were placed general anesthesia (1–2% isoflurane, 0.8–1.0 L/min O_2) at 8 weeks after STZ administration. MR equipment that was used included a Bruker Biospec 7.0 Tesla/30 cm horizontal-bore imaging spectrometer. Anesthetized (2% isoflurane) restrained mice were placed in an MR probe, and their tissues and organs (liver, kidneys, and heart) were localized by MRI. Images were obtained using a Bruker S116 gradient coil (2.0 milliTesla/m/ampere) and a 72-mm quadrature multirung RF coil.

Multiple ^{1}H-MRI slices of tissues and organs in thoracic and abdominal regions (e.g., lungs, heart, liver, kidneys) were taken in the coronal (horizontal) plane using gradient echo multislice (FLASH [Fast Low Angle SHot]); repetition time [TR] 250 ms, echo time [TE] 6 ms, 256 × 256 matrix, two steps per acquisition, 3 × 3 cm^2 field of view [FOV], 1-mm slice thickness) with motion suppression turned on. Mouse tissues were imaged at 0 (precontrast) and at 90–100 min after contrast agent injection. Mice were injected intravenously with anti-DMPO or normal mouse IgG Abs tagged with a biotin-Gd-DTPA-albumin–based contrast agent (200 μL/kg; 1 mg Ab/kg; 0.4 mmol Gd^{+3}/kg) (16–18). T_1-weighted images were obtained using a FISP (Fast Imaging with Steady state Precession) sequence (TR 3.6 ms, TE 1.8 ms, four steps per acquisition, 3 × 3 cm^2 FOV, 1-mm slice thickness, eight segments, scan repetition time 10 s). Pixel-by-pixel relaxation maps were reconstructed from a series of T_1-weighted images using a nonlinear two-parameter fitting procedure. Relative MR signal intensities were calculated for the selected regions of interest (ROIs), and difference images were obtained before and 180 min after injection of the anti-DMPO probe or IgG contrast agent.

In vitro T_1 measurements. Clone 9 normal rat hepatocytes (cultured in 25 cm^2 flasks within complete growth medium to confluency and transferred to serum-free medium 2 h before treatment) were treated with DMPO (40 mmol/L), with hydrogen peroxide (H_2O_2; 50 mmol/L) after 15 min, and then with or without anti-DMPO probe (2 μg) after 30 min (n = 3/group). Cells were incubated with the anti-DMPO probe for an additional 45 min, collected, washed with PBS, and centrifuged (500 rpm for 5 min) to form a pellet for MRI assessment. T_1 values (Bruker Paravision v5.0) were obtained from vial ROIs of T_1-weighted images acquired using rapid acquisition with relaxation enhancement pulse sequence (TE 15 ms, five TRs 200, 400, 800, 1200, 1600 ms, 256 × 256 matrix, two averages, and 1-mm slice thickness). Relaxitivity (mmol/ms) of the anti-DMPO probe was determined to be 9.72 mmol/s, compared with 2.85 mmol/s for Gd-DTPA.

Excised tissues. Diabetic and control mice were injected with DMPO or saline and then with the anti-DMPO molecular probe or with an IgG contrast agent (isotype, molecular-weight control). Liver, kidney, and lung tissues were extracted from anesthetized (isoflurane) mice via abdominal and thoracic incisions made to expose tissues for removal. The extracted tissues (liver, kidneys, and lungs) were cut and fixed in Z-fixative (zinc formalin: formaldehyde 3.7%, zinc sulfate), washed with PBS, and incubated with 15% sucrose before embedding in optimal cutting temperature compound and frozen in liquid nitrogen. Glass slides were prepared with 5- to 8-μm sections and stored at −80°C.

Immunohistochemistry (IHC). To target the anti-DMPO in fixed tissues, cryosections were stained with Cy3-labeled streptavidin, which targets the biotin moiety of the albumin-Gd-DTPA-biotin contrast agent within the excised tissues. An anti-inducible nitric oxide synthase (iNOS) rabbit polyclonal Ab (Santa Cruz Biotech, Inc.) was used to detect iNOS. Stained tissue slices were examined with a Nikon C1 confocal laser scanning microscope (Nikon Instruments, USA). DMPO-MBR nitrone adducts in tissues from control and diabetic animals injected with DMPO or saline were localized using the following procedure: After a rinse in PBS-Tween 20 (washing buffer), the goat anti-DMPO was added in a 1:100 dilution in washing buffer. The goat anti-DMPO Ab was produced against a DMPO-octanoic acid-ovalbumin immunogen at the Ramirez Laboratory in Oklahoma Medical Research Foundation (OMRF). The slides were then incubated overnight at 4°C. After several washes in washing buffer, the secondary Ab donkey anti-goat conjugated to Cy5 (Abcam) was then added in washing buffer (1:250) and incubated for 60 min at room temperature protected from light. After several rinses in washing buffer, ProLong Gold antifade reagent with DAPI (Invitrogen) was used to stain the cell nuclei. After adding DAPI, the slides were covered, sealed, and stored at 4°C and were protected from light until acquisition.

The control slide was rinsed and blocked, as mentioned above, and used to rule out nonspecific secondary Ab binding and endogenous fluorescence. Instead of a primary Ab, the slide was blocked overnight at 4°C in washing buffer or preimmune normal goat serum. After a rinse, two samples from each group on the slide were incubated with the secondary Ab labeled with Cy5, and the other two samples from each group were incubated with washing buffer alone. The incubation was for 60 min at 37°C while protected from light, followed by several rinses in washing buffer. Confocal imaging of the slides was performed at the OMRF Imaging Core Facility using a Zeiss LSM-510META Laser Scanning Confocal Microscope with using a ×60 objective.

Statistical analyses. Statistical differences between the probe administered and control groups were analyzed with an unpaired, two-tailed Student t test by using commercially available InStat software (GraphPad Software, San Diego, CA). For the kinetic study a Spearman correlation (InStat) was done to compare different groups administered the anti-DMPO probe or the nonspecific molecular weight–matched IgG contrast agent. A value of $P < 0.05$ was considered to indicate a statistically significant difference.

RESULTS

MBRs generated during oxidative stress processes in a diabetic mouse model were trapped with the nitrone spin-trapping agent DMPO and subsequently detected in vivo with an mMRI immuno-spin trapping probe targeting DMPO-protein radical adducts. The presence of the anti-DMPO probe in diseased tissues was corroborated using fluorescence imaging and IHC.

mMRI and immuno-spin trapping detection of in vivo protein/lipid radicals. With the use of mMRI and a Gd-based anti-DMPO molecular-targeting probe (see Fig. 1*C*) in an STZ-induced mouse model for diabetes, an increase was found in MR signal intensities in the lungs, livers, and kidneys obtained from T_1-weighted MRIs of severely (Fig. 2*A*) and moderately diabetic mice (Fig. 2*B*), compared with a contrast agent control consisting of nonspecific IgG covalently bound to the Gd-albumin-biotin construct instead of the anti-DMPO Ab (Fig. 2*C*). The difference in images between pre- and 120 min postadministration of the anti-DMPO probe depict highlighted regions in the STZ-treated mouse lungs, kidneys, and livers in moderate and severe diabetes. Expected high levels of the anti–DMPO-probe or IgG-contrast agent are observed in the vascular (heart and major blood vessels), gastrointestinal (stomach and intestines) structures, and the bladder, due to distribution and elimination of the contrast agents. Figure 3 indicates that there are significantly higher percent (%) changes in MR signal intensities in liver (*A*), kidney (*B*), and lung (*C*) of severely diabetic mice (>300 glucose) compared with nondiabetic (*A*, P = 0.0138; *B*, P = 0.0033; *C*, P = 0.0210), non-DMPO (*A*, P = 0.0163; *B*, P = 0.0034; *C*, P = 0.0268), and IgG contrast agent (*A*, P = 0.0163; *B*, P = 0.0039; *C*, P = 0.0284) control mice. In liver ROIs from moderately diabetic (250–300 glucose) STZ-treated mice, relative MR signal intensities (Di), and T_1 (Dii) and T_2 (Diii) relaxation time differences, compared with nondiabetic controls, were significantly higher (P = 0.0171 for relative MR signal intensity; P = 0.0203 for T_1 differences; or P = 0.0073 for

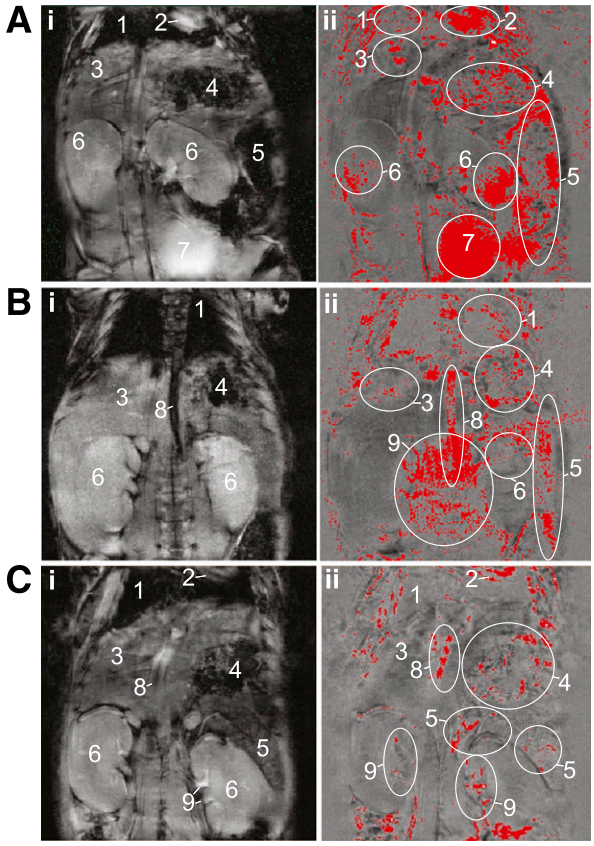

FIG. 2. In vivo MRI of immuno-spin trapped DMPO adducts. *A*: Representative horizontal T_1-weighted MRI from an STZ-induced severely diabetic mouse depicting lungs (*1*: darkened regions), heart (*2*), liver (*3*: gray region: midleft portion of image), stomach (*4*), small and large intestines (*5*), kidneys (*6*: elliptical gray regions: bottom portion of image), and bladder (*7*). Representative precontrast image before anti-DMPO probe (*i*) and postcontrast difference image 180 min after anti-DMPO probe (*ii*). Note increased MR signal intensity (*red*) in difference image within regions of lungs (*1*), liver (*3*), and kidneys (*6*: highlighted with ellipses). Expected increases in vasculature (e.g., heart, *2*), gastrointestinal tract (e.g., stomach, *4*) and small/large intestines (*5*), and bladder (*7*) are outlined. *B*: Representative MRI from a moderately diabetic mouse before (*i*) and difference image 180 min after anti-DMPO probe (*ii*). Increased MR signals in difference image (*ii*) are observed in lungs (*1*), liver (*3*), and kidneys (*6*). Expected increases in signal intensities in vasculature (e.g., major blood vessels, *8*: e.g., aorta and/or vena cava), and renal vasculature (*9*), and gastrointestinal tract (stomach, *4*; and small/large intestines, *5*), are outlined. *C*: Representative MRI from a severely diabetic mouse administered an IgG contrast agent (control). Representative precontrast image before IgG contrast agent (*i*) and postcontrast difference image 180 min after IgG contrast agent (*ii*). Little to no signal is observed in lungs (*1*), liver (*3*), or kidneys (*6*); however, increased signals are observed in the vasculature (heart, *2*; aorta/vena cava, *8*; and renal vasculature, *9*) and the gastrointestinal tract (stomach, *4*; and small and large intestines, *5*). (A high-quality color representation of this figure is available in the online issue.)

T_2 differences). Figure 3*E* specifically illustrates the selective significant elevated uptake of the anti-DMPO probe over the course of 75 min in diabetic mouse livers (P = 0.0154) compared with nondiabetic controls, or the nonspecific uptake of the molecular weight–matched IgG contrast agent in diabetic mouse livers.

In vitro T_1 measurements in hepatocytes. To establish specificity of the anti-DMPO probe in oxidized cells in vitro, clone 9 normal rat hepatocytes were treated with DMPO + H_2O_2 + anti-DMPO probe and found to have mean ± SD T_1 values of 1,283.58 ± 42.86, which were significantly lower (P = 0.0023) than cells with H_2O_2 + DMPO and no anti-DMPO probe (T_1 = 1,464.35 ± 14.66). These oxidized cells with the anti-DMPO probe also had significantly lower T_1 values compared with cells alone (T_1 = 1,551.56 ± 9.77; P = 0.0005).

Fluorescence image detection of protein/lipid radical probe in diabetic tissues. Figure 4 illustrates validation of the presence of the anti-DMPO probe bound to free radical–damaged tissues as detected by the fluorescence labeling of the biotin (see probe illustration in Fig. 1*B*) after in vivo administration of the anti-DMPO probe (intravenous tail vein) and MRI studies. The fluorescence stain (streptavidin conjugated with Cy3) to biotin in the STZ-treated liver, kidneys, and lungs clearly indicates that the Gd-albumin-anti-DMPO agent specifically binds to the injured tissues (representative data presented in Fig. 4*A–C*) compared with the tissues exposed to the IgG control MRI contrast agent (Fig. 4*D–F*; liver, kidneys, and lungs, respectively), which have less fluorescence staining. As expected, fairly high levels of the IgG contrast agent are detected in the kidneys (Fig. 4*E*) due to clearance. The results in Fig. 4*G* confirm the presence of the anti-DMPO probe bound to oxidatively damaged liver tissue in a moderate diabetic mouse (and not in normal liver tissue [control + DMPO]; nondiabetic mouse treated with DMPO; Fig. 4*H*) as detected by the fluorescence labeling of the biotin. The fluorescence stain (Cy3 with streptavidin), which binds to the biotin moiety of the anti-DMPO probe in the STZ-treated liver, clearly indicates that anti-DMPO probe is detected and specifically binds to the injured liver (Fig. 4*G*) compared with control liver tissue (Fig. 4*H*), which has very little fluorescence staining. The tissues for fluorescent staining were obtained from the MRI datasets using spatial coordinates. These results illustrate the feasibility of using molecular-targeted MRI to visualize the in vivo levels of protein radicals trapped by DMPO in a diabetes model.

IHC detection of iNOS in diabetic tissues. Figure 5 illustrates the increased detection of iNOS in diabetic mouse livers (1,438.0 ± 52.8 AU; n = 100) compared with nondiabetic controls (368.1 ± 12.0 AU; n = 93).

IHC detection of DMPO adducts in diabetic tissues. Figure 6 demonstrates the presence of DMPO adducts in nondiabetic and diabetic ex vivo mouse livers (Fig. 6*A* and *B*, respectively) after immuno-spin trapping. The nondiabetic mouse livers have detectable levels of DMPO adducts, but the levels are substantially less than those detected in the diabetic mice.

DISCUSSION

Understanding the underlying role of oxidative stress in diabetes is of paramount importance. Diabetes statistics from the American Diabetes Association (http://www.diabetes.org/diabetes-basics/diabetes-statistics/, 2011) indicate 25.8 million children and adults in the United States (8.3% of the population) have diabetes. Oxidative stress has been implicated as a contributor to the onset and progression of diabetes (1,2), including development of insulin resistance, β-cell dysfunction, impaired glucose tolerance, and mitochondrial dysfunction (19). It has been proposed that there is a mitochondrial production of ROS in response to chronic hyperglycemia. ROS may be the key initiator for each of the pathogenic processes associated with diabetes (20).

The generation of reactive oxygen and nitrogen species, and accumulation of free fatty acids (1,21) leads to lipid peroxidation. The increased free fatty acids, which result in

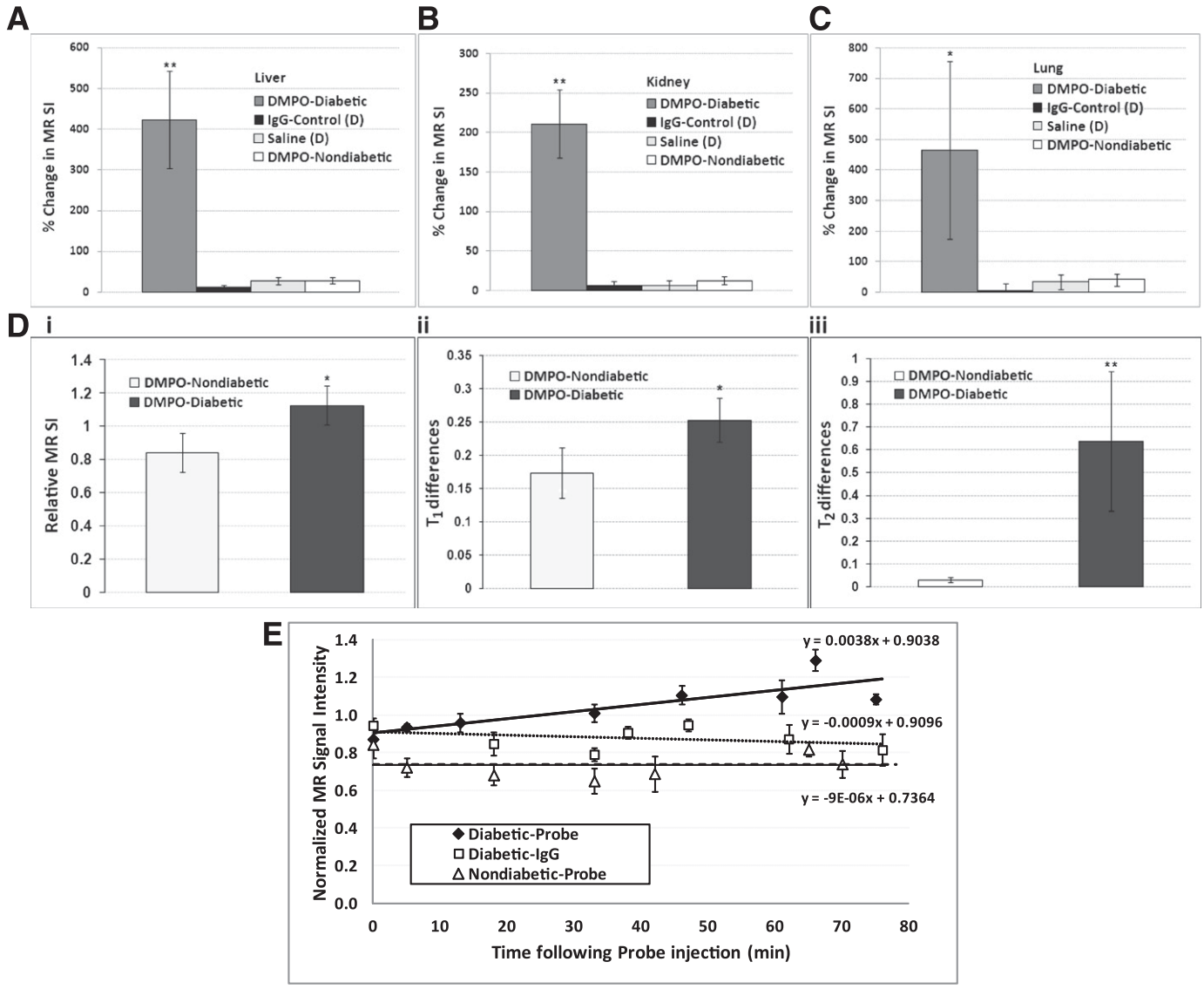

FIG. 3. Quantitative MRI assessment of immuno-spin trapped radicals. Percent (%) change in signal intensity (SI) in liver (*A*), kidney (*B*), and lung (*C*) tissues from STZ-induced diabetic (highly; >300 mg/dL blood glucose) mice (n = 4/group) after being administered DMPO daily for 5 consecutive days and an IgG-albumin-Gd-DTPA contrast agent (nonspecific control) or the anti–DMPO-albumin-Gd-DTPA probe. Significant differences (*P < 0.05 for liver or lung; **P < 0.01 for kidney) were found between mice administered the IgG control and those administered the anti-DMPO probe. *D*: Relative SI (*i*), T_1 (*ii*), and T_2 (*iii*) relaxation differences (significant **P < 0.01 for T_2; *P < 0.05 for relative SI or T_1) between STZ-induced moderately diabetic (250–300 mg/dL blood glucose) mouse livers and nondiabetic mouse livers administered DMPO daily for 5 consecutive days and the anti-DMPO probe. *E*: Kinetic uptake of the anti-DMPO probe (closed diamonds) or nondiabetic (open triangles) mouse livers, or the nonspecific IgG contrast agent in diabetic mouse livers (open squares), over the course of ~70 min, as measured by a normalized (liver tissue ROI divided by muscle tissue ROI; n = 4 for each tissue and each treatment group) MR signal intensity. Only the anti-DMPO probe in diabetic mouse livers is significantly increased (*P < 0.05; Spearman correlation) compared with a nondiabetic control or a diabetic mouse administered the nonspecific IgG-matching molecular weight contrast agent.

lipid peroxidation, then lead to the disruption of membranes, proteins, and DNA (1). Localized tissue oxidative stress is postulated to be a key component in the development of diabetic nephropathy (20). In the kidney, a number of pathways that generate ROS, such as glycolysis, specific defects in the polyol pathway, uncoupling of NOS, xanthine oxidase, NAD(P)H oxidase, and advanced glycation, have been identified to play major roles in the pathogenesis of diabetic kidney disease (13). Excessive oxidative stress in the vasculature is also known to lead to endothelial cell dysfunction and subsequent diabetic nephropathy (22). The microvascular complications in diabetes are thought to be induced by hyperglycemia-associated oxidative stress pathways, including the polyol pathway, advanced glycation end products (AGEs) formation, protein kinase C (PKC)-diacylglycerol (DAG) pathway, and the hexosamine pathway (23). Liver lipoperoxidation (24) and iNOS were also found to increase in STZ-induced diabetic rats (24–26). Oxidative damage to proteins in an STZ-induced diabetes rat model has also been detected in the liver and kidneys, which included iNOS overexpression, lipid radical generation, 4-hydroxynonenal–adducted protein formation, and protein tyrosine nitration (26). Other protein oxidation modifications associated with type 2 diabetes include an increase in carbonyl compounds that correlates with insulin resistance (27) and associated decreases in SOD activity and increases in malondialdehyde (27). Formation of carbonyls has been suggested to be

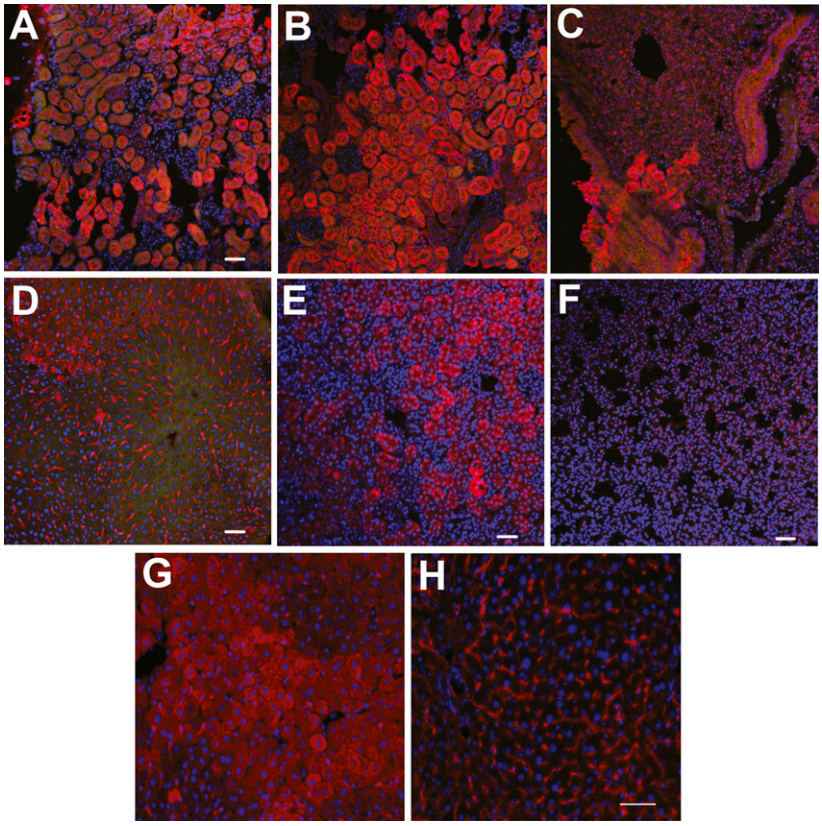

FIG. 4. Fluorescence validation of the presence of anti-DMPO probe in diabetic mouse tissues. Fluorescence detection of the anti-DMPO probe in diabetic (>300 mg/dL blood glucose) mouse liver (*A*), kidney (*B*), and lung (*C*) tissues compared with those administered an IgG contrast agent in diabetic mouse liver (*D*), kidney (*E*), and lung (*F*) tissues. Fluorescence detection of anti-DMPO probes in an STZ-induced moderately diabetic (250–300 mg/dL blood glucose) mouse liver at 8 weeks after STZ administration (*G*), and a control nondiabetic mouse liver (*H*). The anti-DMPO mMRI probe was detected using a SA-Cy5 complex and the nuclei were stained with DAPI. Scale bars are 50 μm. (A high-quality color representation of this figure is available in the online issue.)

mediated by formation of a transient protein-centered radical in human albumin treated with a Fenton-like reagent (Cu^{2+}/H_2O_2) (28).

MR techniques have been used in the past few decades to assess various pathologies associated with diabetes. For instance, cine MRI is a complimentary imaging tool, along with Doppler ultrasound imaging, which is used to assess diastolic cardiac function in diabetes. We have previously used cine MRI to demonstrate within an STZ-induced diabetic mouse model at 4 weeks after STZ induction that there are significant deficits in myocardial morphology and function, including decreased left ventricular (LV) wall thickness, increased LV end-systolic diameter and volume, diminished LV ejection fraction and cardiac output, decreased LV circumferential shortening, and decreased LV peak ejection and filling rates (29). Others have used contrast-enhanced MRI with a long circulating paramagnetic contrast agent, protected copolymer (PGC) covalently linked to Gd-DTPA labeled with fluorescein isothiocyanate (PGC-Gd-DTPA-F), to assess vascular alterations in the pancreas of STZ-induced diabetic mice (30). Other diabetes-related studies have incorporated magnetically labeled (cross-linked iron oxide [CLIO]-particles coupled with Tat; CLIO-Tat) cytotoxic lymphocytes with mMRI to assess the autoimmune destruction of insulin-producing pancreatic β-cells in mice (31). Iron oxide-based contrast agents have also been used to label pancreatic islets and access their survival after transplantation (32).

Ab-targeted delivery of contrast agents has been incorporated to enhance the sensitivity and accuracy of MRI. Our laboratory, for example, has used mMRI methodology to provide in vivo evidence regarding the overexpression of the tumor marker c-Met (16), the angiogenesis marker vascular endothelial growth factor receptor 2 (17), and iNOS (18) in rodent models for gliomas. A similar approach, coupled with immuno-spin trapping, was used in this study to detect MBRs in oxidative stress-related diseases. mMRI provides the advantage of image resolution, as well as the assessment of the spatial location of in vivo oxidative stress events, coupled with immuno-spin trapping, in heterogeneous tissues or organs.

MBRs can be trapped by the spin-trapping compound, DMPO, to form paramagnetic DMPO-MBR adducts, which can be detected by electron spin resonance (ESR) spectroscopy. These adducts, however, decay in a few minutes to an ESR-silent (undetectable) nitrone. With the use of immuno-spin trapping, the nitrone MBR adduct can be studied by using an Ab against the DMPO-nitrone adduct (11,28,33–35). Specifically, in this study we used a probe that can detect in vivo levels of MBR that were trapped by DMPO and subsequently targeted with a MRI-observable anti-DMPO probe, which consisted of an anti-DMPO Ab that targets the DMPO-MBR adducts, and a Gd-albumin–based MRI contrast agent. Predominantly, protein radical detection has been reported with immune-spin trapping in the past (15,33,34,36). In at least one account, this method

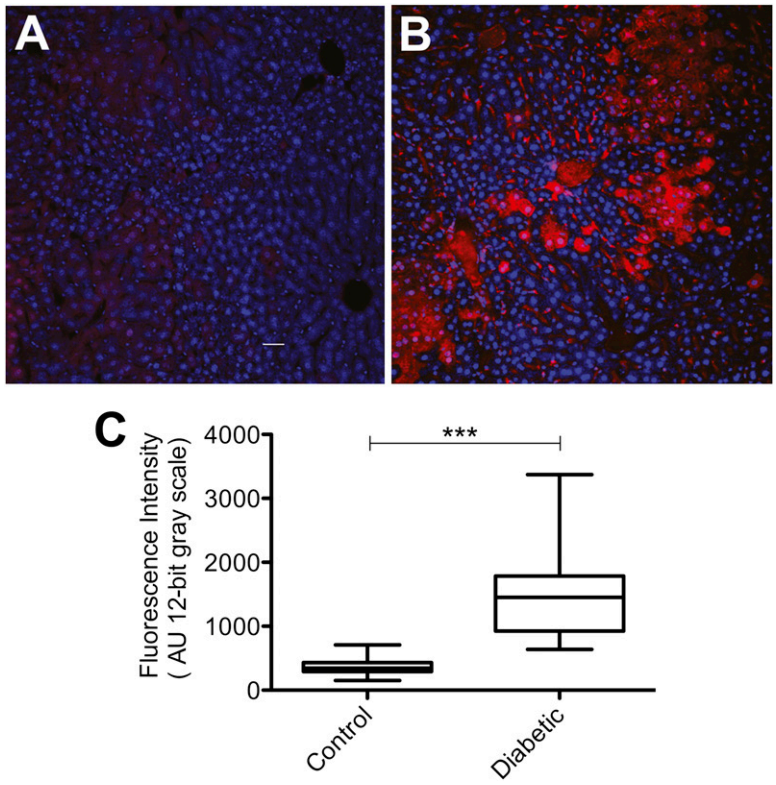

FIG. 5. IHC staining for iNOS in control (nondiabetic) livers (*A*) and diabetic mouse livers (*B*). *C*: Quantification of the fluorescence intensity (AU 12-bit scale) in control and diabetic mouse liver tissue samples, with a significant increase (*$P < 0.0001$) in the diabetic samples compared with controls. The horizontal line in the middle of each box indicates the median; the top and bottom borders of the box mark the 75th and 25th percentiles, respectively, and the whiskers mark the 90th and 10th percentiles. (A high-quality color representation of this figure is available in the online issue.)**

was used to trap free radicals in the plasma membrane (36). DMPO has been previously used to trap lipid radicals (37–39), and some of the MBR being trapped are possibly of lipid origin. It is interesting to note that albumin-coated nanoparticles may be taken up into cells via the caveolae (40), which may allow the albumin-based anti-DMPO probe to trap intracellular radicals, although this concept would need to be further studied.

The mMRI method coupled with the use of an anti-DMPO probe specific for DMPO-MBR adducts allowed the specific detetion of the presence of MBR in lung, liver, and kidney tissues of mice with severe and moderate diabetes (Figs. 2 and

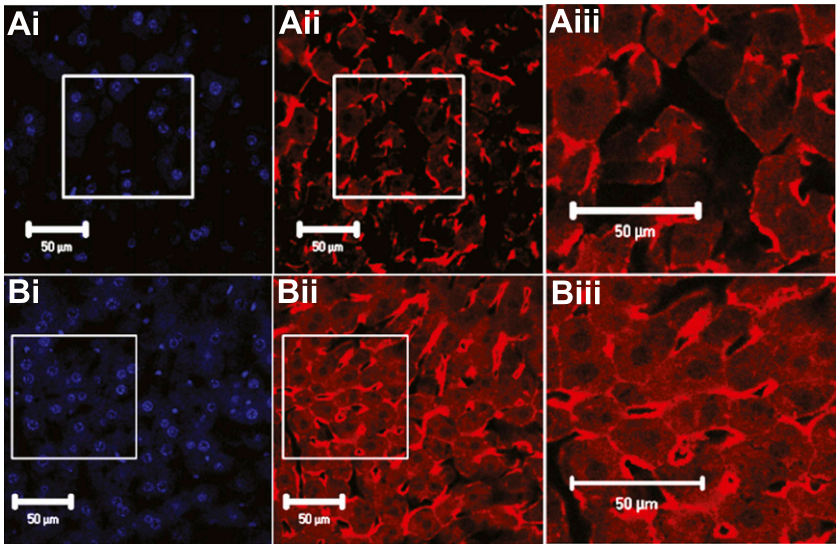

FIG. 6. IHC validation of DMPO adducts in diabetic mouse livers. Fluorescence detection of DMPO adducts in (*A*) nondiabetic and (*B*) diabetic mouse livers. Blue (DAPI) stain for cell nuclei (*i*). A goat anti-DMPO was used to detect DMPO-nitrone adducts and a donkey anti-goat IgG conjugated to Cy5 (Aves) was used to localize the immunocomplexes formed (red fluorescence) (*ii*). Enlarged regions from selected areas are shown in *ii* (*iii*). Nondiabetic mouse livers have some DMPO adducts in extracellular spaces. Diabetic mice have increased intracellular DMPO adducts, as well as within extracellular spaces. (A high-quality color representation of this figure is available in the online issue.)

3) at 50 μm in-plane resolution. Previous studies clearly show that lung (41–43), kidney (6,20,22,26,44,45), and liver (6,24–26,46) tissues are severely affected in diabetes models. Selective uptake of the anti-DMPO probe in diabetic mouse livers is illustrated in Fig. 3*E*. In comparison, EPR imaging provides low image resolution due to broad spectral line widths, although sensitivity may be higher. To corroborate the localization of the anti-DMPO probe in tissues of diabetic and control animals, we used fluorescence imaging by targeting the biotin moiety of the anti-DMPO probe with streptavidin-Cy3, which clearly showed elevated levels of the anti-DMPO probe in diabetic tissues, particularly the liver and lungs (Fig. 4). IHC was used to detect and quantify elevated levels of iNOS in ex vivo diabetic mouse liver tissue samples, compared with nondiabetic controls (Fig. 5), as iNOS levels have been previously shown to be correlated with diabetes severity in liver (25,26) and kidneys (26,47). IHC was used to confirm the presence of ex vivo DMPO adducts in diabetic mouse livers by using a Cy5-secondary Ab that recognizes the goat anti-DMPO Ab (Fig. 6). In vitro specificity of anti-DMPO in oxidized cells was established by measuring T_1 values of clone 9 hepatocytes with H_2O_2 and DMPO. Oxidized cells with the anti-DMPO probe were found to have a significant decrease in T_1 compared with cells with H_2O_2 and DMPO without the anti-DMPO probe, or cells alone, thus confirming the binding of the anti-DMPO probe on oxidized cells with DMPO-radical adducts.

This is the first report of whole-body imaging of in vivo MBRs. Although we reported the use of a MRI-visible anti-DMPO probe to detect DMPO adducts of MBR in tissues with diabetes complications, this method could also be invaluable in assessing MBR damage in multiple tissue and organ pathologies associated with various oxidative stress-related diseases in preclinical models.

ACKNOWLEDGMENTS

The OMRF, the National Institute of Environmental Health Sciences (to R.M.), and the National Institutes of Health IDeA Networks of Biomedical Research Excellence (Grant P20-RR-016478-09 to R.A.T.) provided funds that contributed to this study.

No potential conflicts of interest relevant to this article were reported.

R.A.T. conceived of the study idea, oversaw all aspects of the project, analyzed and interpreted the results, and wrote the manuscript. N.S. synthesized and characterized the anti-DMPO probe. D.S. treated animals with STZ and DMPO and prepared animals for MRI experiments. M.H. and K.D. obtained and analyzed the MRI data. F.L. and R.S.-M. obtained and interpreted the fluorescence imaging data for validation of the presence of the bound protein/lipid radical probe in tissues. D.C.R. and S.E.G.-M. obtained the immunohistochemistry fluorescence images confirming the formation of DMPO-protein/lipid radicals with immuno-spin trapping. M.G.B., M.E., and R.P.M. obtained, characterized, and provided the anti-DMPO Abs that were used to generate the anti-DMPO mMRI probe and immuno-spin trapping validation studies. R.A.T. is the guarantor of this work and, as such, had full access to all the data in the study and takes responsibility for the integrity of the data and the accuracy of the data analysis.

REFERENCES

1. West IC. Radicals and oxidative stress in diabetes. Diabet Med 2000;17:171–180
2. Lenzen S. Oxidative stress: the vulnerable beta-cell. Biochem Soc Trans 2008;36:343–347
3. Francia P, Cosentino F, Schiavoni M, et al. p66(Shc) protein, oxidative stress, and cardiovascular complications of diabetes: the missing link. J Mol Med (Berl) 2009;87:885–891
4. Tabak O, Gelisgen R, Erman H, et al. Oxidative lipid, protein, and DNA damage as oxidative stress markers in vascular complications of diabetes mellitus. Clin Invest Med 2011;34:E163–E171
5. Gunnarsson R, Berne C, Hellerström C. Cytotoxic effects of streptozotocin and N-nitrosomethylurea on the pancreatic B cells with special regard to the role of nicotinamide-adenine dinucleotide. Biochem J 1974;140:487–494
6. Portero-Otín M, Pamplona R, Ruiz MC, Cabiscol E, Prat J, Bellmunt MJ. Diabetes induces an impairment in the proteolytic activity against oxidized proteins and a heterogeneous effect in nonenzymatic protein modifications in the cytosol of rat liver and kidney. Diabetes 1999;48:2215–2220
7. Matsumoto K, Hyodo F, Anzai K, Utsumi H, Mitchell JB, Krishna MC. Brain redox imaging. Methods Mol Biol 2011;711:397–419
8. Caia GL, Efimova OV, Velayutham M, et al. Organ specific mapping of in vivo redox state in control and cigarette smoke-exposed mice using EPR/NMR co-imaging. J Magn Reson 2012;216C:21–27
9. Hirayama A, Nagase S. Electron paramagnetic resonance imaging of oxidative stress in renal disease. Nephron Clin Pract 2006;103:c71–c76
10. Sonta T, Inoguchi T, Matsumoto S, et al. In vivo imaging of oxidative stress in the kidney of diabetic mice and its normalization by angiotensin II type 1 receptor blocker. Biochem Biophys Res Commun 2005;330:415–422
11. Burks SR, Legenzov EA, Rosen GM, Kao JP. Clearance and biodistribution of liposomally encapsulated nitroxides: a model for targeted delivery of electron paramagnetic resonance imaging probes to tumors. Drug Metab Dispos 2011;39:1961–1966
12. Hall AM, Crawford C, Unwin RJ, Duchen MR, Peppiatt-Wildman CM. Multiphoton imaging of the functioning kidney. J Am Soc Nephrol 2011;22:1297–1304
13. Qin LX, Ma W, Li DW, et al. Coenzyme Q functionalized CdTe/ZnS quantum dots for reactive oxygen species (ROS) imaging. Chemistry 2011;17:5262–5271
14. Keshari KR, Kurhanewicz J, Bok R, Larson PE, Vigneron DB, Wilson DM. Hyperpolarized ^{13}C dehydroascorbate as an endogenous redox sensor for in vivo metabolic imaging. Proc Natl Acad Sci U S A 2011;108:18606–18611
15. Mason RP. Using anti-5,5-dimethyl-1-pyrroline N-oxide (anti-DMPO) to detect protein radicals in time and space with immuno-spin trapping. Free Radic Biol Med 2004;36:1214–1223
16. Towner RA, Smith N, Doblas S, et al. In vivo detection of c-Met expression in a rat C6 glioma model. J Cell Mol Med 2008;12:174–186
17. He T, Smith N, Saunders D, et al. Molecular MRI assessment of vascular endothelial growth factor receptor-2 in rat C6 gliomas. J Cell Mol Med 2011;15:837–849
18. Towner RA, Smith N, Doblas S, et al. In vivo detection of inducible nitric oxide synthase in rodent gliomas. Free Radic Biol Med 2010;48:691–703
19. Rains JL, Jain SK. Oxidative stress, insulin signaling, and diabetes. Free Radic Biol Med 2011;50:567–575
20. Forbes JM, Coughlan MT, Cooper ME. Oxidative stress as a major culprit in kidney disease in diabetes. Diabetes 2008;57:1446–1454
21. Sugimoto R, Enjoji M, Kohjima M, et al. High glucose stimulates hepatic stellate cells to proliferate and to produce collagen through free radical production and activation of mitogen-activated protein kinase. Liver Int 2005;25:1018–1026
22. Singh DK, Winocour P, Farrington K. Oxidative stress in early diabetic nephropathy: fueling the fire. Nat Rev Endocrinol 2011;7:176–184
23. Madonna R, De Caterina R. Cellular and molecular mechanisms of vascular injury in diabetes—part I: pathways of vascular disease in diabetes. Vascul Pharmacol 2011;54:68–74
24. Di Naso FC, Simões Dias A, Porawski M, Marroni NA. Exogenous superoxide dismutase: action on liver oxidative stress in animals with streptozotocin-induced diabetes. Exp Diabetes Res 2011;2011:754132
25. Khandelwal RL, Gupta D, Sulakhe PV. Decreased activity and impaired induction of nitric oxide synthase by lipopolysaccharides in streptozotocin-induced diabetic rats. Biochim Biophys Acta 2003;1620:259–266
26. Stadler K, Bonini MG, Dallas S, et al. Involvement of inducible nitric oxide synthase in hydroxyl radical-mediated lipid peroxidation in streptozotocin-induced diabetes. Free Radic Biol Med 2008;45:866–874
27. Huang X, Sun M, Li D, et al. Augmented NADPH oxidase activity and p22phox expression in monocytes underlie oxidative stress of patients with type 2 diabetes mellitus. Diabetes Res Clin Pract 2011;91:371–380
28. Ramirez DC, Mejiba SE, Mason RP. Copper-catalyzed protein oxidation and its modulation by carbon dioxide: enhancement of protein radicals in cells. J Biol Chem 2005;280:27402–27411

29. Yu X, Tesiram YA, Towner RA, et al. Early myocardial dysfunction in streptozotocin-induced diabetic mice: a study using in vivo magnetic resonance imaging (MRI). Cardiovasc Diabetol 2007;6:6
30. Medarova Z, Castillo G, Dai G, Bolotin E, Bogdanov A, Moore A. Noninvasive magnetic resonance imaging of microvascular changes in type 1 diabetes. Diabetes 2007;56:2677–2682
31. Moore A, Sun PZ, Cory D, Högemann D, Weissleder R, Lipes MA. MRI of insulitis in autoimmune diabetes. Magn Reson Med 2002;47:751–758
32. Medarova Z, Moore A. MRI as a tool to monitor islet transplantation. Nat Rev Endocrinol 2009;5:444–452
33. Ramirez DC, Gomez-Mejiba SE, Corbett JT, Deterding LJ, Tomer KB, Mason RP. Cu,Zn-superoxide dismutase-driven free radical modifications: copper- and carbonate radical anion-initiated protein radical chemistry. Biochem J 2009;417:341–353
34. Ranguelova K, Chatterjee S, Ehrenshaft M, et al. Protein radical formation resulting from eosinophil peroxidase-catalyzed oxidation of sulfite. J Biol Chem 2010;285:24195–24205
35. Chatterjee S, Lardinois O, Bhattacharjee S, et al. Oxidative stress induces protein and DNA radical formation in follicular dendritic cells of the germinal center and modulates its cell death patterns in late sepsis. Free Radic Biol Med 2011;50:988–999
36. Bonini MG, Siraki AG, Atanassov BS, Mason RP. Immunolocalization of hypochlorite-induced, catalase-bound free radical formation in mouse hepatocytes. Free Radic Biol Med 2007;42:530–540
37. Chamulitrat W, Jordan SJ, Mason RP. Fatty acid radical formation in rats administered oxidized fatty acids: in vivo spin trapping investigation. Arch Biochem Biophys 1992;299:361–367
38. Dikalov SI, Mason RP. Spin trapping of polyunsaturated fatty acid-derived peroxyl radicals: reassignment to alkoxyl radical adducts. Free Radic Biol Med 2001;30:187–197
39. Reis A, Domingues P, Ferrer-Correia AJ, Domingues MR. Identification of free radicals of glycerophosphatidylcholines containing omega-6 fatty acids using spin trapping coupled with tandem mass spectrometry. Free Radic Res 2007;41:432–443
40. Wang Z, Tiruppathi C, Minshall RD, Malik AB. Size and dynamics of caveolae studied using nanoparticles in living endothelial cells. ACS Nano 2009;3:4110–4116
41. Eren G, Cukurova Z, Hergunsel O, et al. Protective effect of the nuclear factor kappa B inhibitor pyrrolidine dithiocarbamate in lung injury in rats with streptozotocin-induced diabetes. Respiration 2010;79:402–410
42. Oztay F, Kandil A, Gurel E, et al. The relationship between nitric oxide and leptin in the lung of rat with streptozotocin-induced diabetes. Cell Biochem Funct 2008;26:162–171
43. Spadella CT, Suarez OA, Lucchesi AN, Marques SF, Cataneo AJ. Effects of pancreas transplantation on oxidative stress in pulmonary tissue from alloxan-induced diabetic rats. Transplant Proc 2010;42:2087–2091
44. Noh H, Oh EY, Seo JY, et al. Histone deacetylase-2 is a key regulator of diabetes- and transforming growth factor-beta1-induced renal injury. Am J Physiol Renal Physiol 2009;297:F729–F739
45. Zheng H, Whitman SA, Wu W, et al. Therapeutic potential of Nrf2 activators in streptozotocin-induced diabetic nephropathy. Diabetes 2011;60:3055–3066
46. George N, Peeyush Kumar T, Antony S, Jayanarayanan S, Paulose CS. Effect of vitamin D3 in reducing metabolic and oxidative stress in the liver of streptozotocin-induced diabetic rats. Br J Nutr 2012;6:1–9
47. Yokozawa T, Cho EJ, Park CH, Kim JH. Protective effect of proanthocuyanidin against diabetic oxidative stress. Evid Based Complement Alternat Med 2012;2012:623879